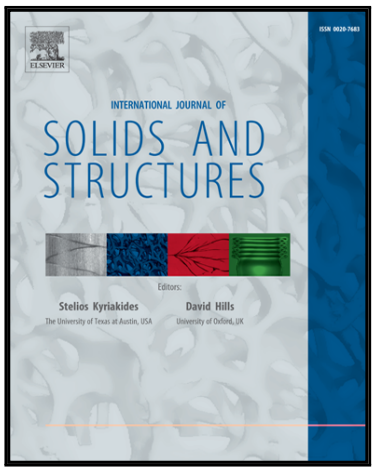

Perturbation-based Stochastic Multi-scale Computational Homogenization Method for Woven Textile Composites

X.-Y. Zhou, P.D. Gosling, C.J. Pearce, Z. Ullah, L. Kaczmarczyk

PII: S0020-7683(15)00392-3
DOI: 10.1016/j.ijsolstr.2015.09.008
Reference: SAS 8903

To appear in: *International Journal of Solids and Structures*

Received date: 15 April 2015
Revised date: 19 August 2015
Accepted date: 7 September 2015

Please cite this article as: X.-Y. Zhou, P.D. Gosling, C.J. Pearce, Z. Ullah, L. Kaczmarczyk, Perturbation-based Stochastic Multi-scale Computational Homogenization Method for Woven Textile Composites, *International Journal of Solids and Structures* (2015), doi: 10.1016/j.ijsolstr.2015.09.008

Highlights

- A stochastic homogenization method is proposed for the prediction of statistics of effective material properties for textile composites.
- Finite element implementation procedure is given for the computational multi-scale homogenisation method.
- The statistics of effective elastic properties are obtained using the perturbation-based method.
- The proposed methodology is validated through numerical study.

Perturbation-based Stochastic Multi-scale Computational Homogenization Method for Woven Textile Composites

X.-Y. Zhou[a], P. D. Gosling[a,*], C. J. Pearce[b], Z. Ullah[b], L. Kaczmarczyk[b]

[a]*School of Civil Engineering & Geosciences, Newcastle University, Newcastle upon Tyne, NE1 7RU, UK.*
[b]*School of Engineering, University of Glasgow, Glasgow, G12 8QQ, UK*

Abstract

In this paper, a stochastic homogenization method that couples the state-of-the-art computational multi-scale homogenization method with the stochastic finite element method, is proposed to predict the statistics of the effective elastic properties of textile composite materials. Uncertainties associated with the elastic properties of the constituents are considered. Accurately modelling the fabric reinforcement plays an important role in the prediction of the effective elastic properties of textile composites due to their complex structure. The p-version finite element method is adopted to refine the analysis. Performance of the proposed method is assessed by comparing the mean values and coefficients of variation for components of the effective elastic tensor obtained from the present method against corresponding results calculated by using Monte Carlo simulation method for a plain-weave textile

*Corresponding author
Email addresses: xiaoyi.zhou@newcastle.ac.uk (X.-Y. Zhou), p.d.gosling@newcastle.ac.uk (P. D. Gosling), chris.pearce@glasgow.ac.uk (C. J. Pearce), zahur.ullah@glasgow.ac.uk (Z. Ullah), lukasz.kaczmarczyk@glasgow.ac.uk (L. Kaczmarczyk)

composite. Results show that the proposed method has sufficient accuracy to capture the variability in effective elastic properties of the composite induced by the variation of the material properties of the constituents.

Keywords: textile composites; effective elastic properties; computational multi-scale homogenization method; stochastic finite element method.

1. Introduction

Composites are increasingly popular in civil engineering due to their ability to fulfil demands where conventional materials such as concrete and steel can not meet engineering requirements, including long term durability or extreme large clear span/space. Among composites, textile composites are preferable due to their low material costs and labour requirements compared to traditional unidirectional prepreg composites. Understanding the mechanical behaviour of composites is the primary step, and critical in the design of composite structures. However, several factors, such as fibre yarn and matrix properties, weaving/braiding architecture, yarn spacing (width) and thickness (height), fibre packing density in the yarns, and overall fibre volume fraction, influence the mechanical performance of fabric composites. Furthermore, it is fundamental that uncertainty quantification forms a key component of the structural assessment process. Probabilistic-based methods are powerful tools in structural design to enable consideration of uncertainties in the variability of the mechanical properties.

Homogenization methods have proven to be capable of predicting the mechanical properties of composites, and to be an efficient alternative to time consuming and labour intensive experimental methods, particularly for

complex architectures represented textile fabrics. The most extensively used homogenization methods for textile composites are analytical in nature. A family of methods has been based on the fundamental works of Ishikawa and Chou (1982) and Chou and Ishikawa (1983) where three 1D analytical models for 2D woven composites, including 'mosaic', 'fiber crimp' and 'bridging' models, were developed. Subsequently, these methods were extended by Naik (1994) to consider two-dimensional crimp, in which the yarns of the woven/braided fabrics were divided into slices using parallel planes perpendicular to the fabric plane and along the fibre/yarn direction. To overcome the limitations of 2D models for estimating through-thickness properties (transverse moduli, E_{33}, G_{13} and Poisson's ratio ν_{13} and ν_{23}), a 3D model was proposed by Vandeurzen et al. (1996). In the 1990s and early 2000s, extensive efforts were devoted to improve the performance of these models in predicting effective mechanical properties of textile composites (Sankar and Marrey, 1997; Scida et al., 1999; Ivanov and Tabiei, 2001). A key assumption of the analytical methods is the iso-strain, iso-stress or mixed iso-strain/iso-stress boundary conditions that is used to assemble different material phases in order to predict the overall material properties. However, one important limitation of this assumption is the fact that it does not consider the mechanical interaction among the different solid phases. It is a well known fact that the strain field near the interface between different solid phases can be complex and may have a crucial impact on the macroscopic response.

More sophisticated asymptotic homogenization methods have been introduced. Gommers et al. (1998) applied the classic Mori-Tanaka method to predict the effective elastic properties of various types of woven, knitted

and braided fabric composites. Carvelli and Poggi (2001) and Peng and Cao (2002) proposed a dual homogenization method that estimates yarn properties by microscale to mesoscale homogenization and textile composite properties by mesoscale to macroscale homogenization. The asymptotic homogenization approach provides effective overall properties as well as local stress and strain values. However, considerations are usually restricted to very simple microscopic geometries and simple material models, mostly at small strains.

In the last decade, the computational homogenization has been extensively developed to exploit its performance at predicting the constitutive properties of heterogeneous materials with arbitrary microscopic geometry and constituent behaviours (Michel et al., 1999; Kouznetsova et al., 2001; Miehe and Koch, 2002; Kaczmarczyk et al., 2008; Perić et al., 2011). The method has been successfully applied to the estimation of the effective properties of composites, but applications to textile composites are relatively scarce (Stig and Hallstrm, 2012; Gager and Pettermann, 2012; Fillep et al., 2013).

It is worth mentioning that these well established homogenization schemes are based on the assumption that the mechanical properties of constituent materials are deterministic. Arising from various sources such as manufacturing process, assembly, and quality control limits, composite materials exhibit uncertainties in their material properties, geometry, and fibre volume fractions, as examples (Sriramula and Chryssanthopoulos, 2009). Taking these uncertainties into account in designing composite structures, such as through the use of reliability-based structural design, is essential to ensure that the

structures perform with sufficient safety during their service. A primary task is to determine how these uncertainties affect mechanical behaviour, structural response, and structural performance. In the present study, we will consider the influence of uncertainties in the material properties of the composite constituents on the effective macroscopic material properties. The stochastic finite element method is one of the more widely used methods to quantify uncertainty (Matthies, 2007). Kamiński and Kleiber (2000) proposed a perturbation-based stochastic finite element method (PSFEM) based homogenization method to undertake the stochastic analysis of composite materials with randomness in Young's modulus. Sakata et al. (2008b) extended the perturbation-based method to consider both randomness in Young's modulus and Poisson's ratio, and Sakata et al. (2008a) considered the effect of uncertainty in the fibre volume fraction by using an equivalent inclusion method. To obtain higher order moments, for example skewness and kurtosis, Kamiński (2007) developed a generalized perturbation-based stochastic finite element that is able to consider up to 10th order expansion. The spectral stochastic finite element method (SSFEM) uses the Karhurn-Loève expansion to discretize input of known random fields, and a polynomial chaos expansion to represent the response of unknown random fields such as displacement in solving standard stochastic elastic problem (Ghanem and Spanos, 2003). Homogenization theory is combined with the SSFEM to consider the influence of uncertainties associated with the constituent material properties on the effective material properties for unidirectional composites (Tootkaboni and Graham-Brady (2010)) or nonlinear composite materials (Clément et al., 2013), and geometric uncertainty (Clément et al., 2012).

In almost all the existing studies, the stochastic finite element based uncertainty quantification methods are applied to investigate relatively simple unidirectional composites with constituents comprising isotropic materials, whereas corresponding research on woven textile composite is seldom found. Due to the complex geometry of the fabric and the waviness of the yarn, the influence of uncertainties in the microscopic material properties on the effective elastic properties may differ from those identified in unidirectional fibre reinforced composites. Furthermore, commonly used reinforcements, e.g. graphite fibre, are transversely isotropic or orthotropic, requiring 5 or 9 independent material constants, and the composites may comprise more than two material phases. For instance the warp and weft tows may have different material properties. These features introduce a greater number of random variables, meaning that the PSFEM method may be more efficient than SSFEM in such cases due to the description of the stochastic function (Sudret and Der Kiureghian, 2000; Spanos and Kontsos, 2008).

In order to take the variability of material properties in meso-scale constituents into consideration when predicting the effective elastic properties of woven textile composite, a stochastic homogenization method is developed by integrating the stochastic finite element method with a multi-scale computational homogenization method. The computational homogenization framework presented in (Michel et al., 1999; Kouznetsova et al., 2001; Perić et al., 2011), and the perturbation based stochastic finite element method presented in (Kleiber and Hien, 1992) and (Kamiński, 2013) are used as the basis to develop a perturbation based stochastic multi-scale finite element method (PSMFE). The first step of the method relies on the construction

of a probabilistic model of the microstructure. We then use the unified approach proposed by Kaczmarczyk et al. (2008) to impose the boundary conditions. Finally, we use the perturbation technique to approximate the stochastic function via a Taylor series expansion. The proposed approach is implemented in an in-house finite element modelling software MoFEM (Kaczmarczyk et. al., 2014). The accuracy and the computational efficiency of the developed formulation are demonstrated through numerical studies on a plain-weave textile composite.

2. Multi-scale computational homogenization theory

The computational homogenization method seeks to determine the macroscopic material properties based on the mechanics of the underlying microstructure. There are three important assumptions: (i) the characteristic size of the microstructure is small compared to that of the macrostructure; (ii) the volume average of the microscopic stress/strain must be equal to the macroscopic stress/strain; (iii) the volume average of the microscopic strain power must be equal to the macroscopic strain power (so called Hill-Mandel condition). For a textile composite, the computational homogenization can be realised in five steps: (1) Define the geometry of the Representative Volume Element (RVE); (2) Discretise the RVE and assignment of material properties; (3) Apply a given macrostrain to the RVE using appropriate boundary conditions; (4) Solve RVE boundary value problem; (5) Determine the effective macroscopic properties using the volume averaging theorem. Details of the computational homogenization method for heterogeneous materials adopted in this work can be found in (Michel et al., 1999; Kouznetsova

et al., 2001; Perić et al., 2011; Kaczmarczyk et al., 2008). In what follows we briefly present this computational homogenization scheme for determining the effective elastic properties of a linear elastic textile composite with a suitably described RVE structure undergoing small strains following the notation adopted by Perić et al. (2011).

Let $\mathbf{x}$ be the position of a point in the macro-continuum, and an associated RVE be well defined in geometry. The domain of the RVE, Ω_μ, is assumed to consist in general of a solid part, Ω_μ^s, and a void part Ω_μ^v: $\Omega_\mu = \Omega_\mu^s \cup \Omega_\mu^v$. For composites, the solid part consists of constituents of matrix, Ω_μ^m, and of reinforcement Ω_μ^r: $\Omega_\mu^s = \left(\cup_{i=1}^{k} \Omega_\mu^{m,i}\right) \cup \left(\cup_{j=1}^{l} \Omega_\mu^{r,j}\right)$ with k denoting the number of different matrices in the composite (usually 1) and l representing the number of different fibre types (not infrequently 2, with glass and carbon combined in the same composite). The multiscale structure is schematically illustrated in Fig. 1 for textile composite.

2.1. Macro-to-micro transition

For a given macroscopic strain $\bar{\boldsymbol{\varepsilon}}$, the displacement field within the RVE associated with a point $\mathbf{x}$ in the macro-continuum is defined as

$$\mathbf{u}_\mu(\mathbf{y}) = \bar{\boldsymbol{\varepsilon}}(\mathbf{x})\mathbf{y} + \tilde{\mathbf{u}}_\mu(\mathbf{y}), \quad \mathbf{u}_\mu \in \mathscr{K}_\mu \tag{1}$$

which is a sum of a linear displacement, $\bar{\boldsymbol{\varepsilon}}\mathbf{y}$, and a displacement fluctuation, $\tilde{\mathbf{u}}_\mu$. $\mathscr{K}_\mu$ is the kinematically admissible displacement filed of the RVE. In the following, $\mathbf{y}$ denotes the local coordinate of the RVE, and the microscopic terms are described with subscript μ.

The microscopic strain field within the RVE is the symmetric part of the spatial gradient of the microscopic displacement field and can be expressed

as

$$\boldsymbol{\varepsilon}_\mu(\mathbf{y}) = \nabla_y^s \mathbf{u}_\mu = \bar{\boldsymbol{\varepsilon}}(\mathbf{x}) + \tilde{\boldsymbol{\varepsilon}}_\mu(\mathbf{y}) \tag{2}$$

where where ∇_y^s denotes the symmetric gradient operator with respect to the microscopic coordinates and the microscopic strain fluctuation field is

$$\tilde{\boldsymbol{\varepsilon}}_\mu = \nabla_y^s \tilde{\mathbf{u}}_\mu. \tag{3}$$

Let us assume that the RVE domain Ω_μ contains perfectly bonded phases, the average strain theorem is thus applicable and the volume average of the microscopic strain yields

$$\bar{\boldsymbol{\varepsilon}}(\mathbf{x}) \equiv \frac{1}{V_\mu}\int_{\Omega_\mu} \boldsymbol{\varepsilon}_\mu(\mathbf{y}) dV = \bar{\boldsymbol{\varepsilon}}(\mathbf{x}) + \frac{1}{V_\mu}\int_{\Omega_\mu} \tilde{\boldsymbol{\varepsilon}}_\mu(\mathbf{y}) dV. \tag{4}$$

where $V_\mu = \|\Omega_\mu\|$ is the volume of the RVE. The identity Eq.(4) implies that the estimate of the microscopic strain $\tilde{\boldsymbol{\varepsilon}}_\mu$, or the displacement fluctuation $\tilde{\mathbf{u}}_\mu$, needs to satisfy the constraint

$$\int_{\Omega_\mu} \tilde{\boldsymbol{\varepsilon}}_\mu(\mathbf{y}) dV = \int_{\Omega_\mu} \nabla_y^s \tilde{\mathbf{u}}_\mu(\mathbf{y}) dV = \mathbf{0}. \tag{5}$$

2.2. Micro-to-macro transition

The principle of virtual work establishes that the RVE is in equilibrium if, and only if, the variational equation

$$\int_{\Omega_\mu} \boldsymbol{\sigma}_\mu(\mathbf{y}) : \nabla_y^s \boldsymbol{\eta} dV - \int_{\partial\Omega_\mu} \mathbf{t}^e \cdot \boldsymbol{\eta} dA = 0 \quad \forall \boldsymbol{\eta} \in \mathscr{V}_\mu \tag{6}$$

holds, where $\mathscr{V}_\mu$ is an appropriate space of virtual kinematically admissible displacement field of the RVE, $\boldsymbol{\eta}$ is virtual displacement field, and $\mathbf{t}^e$ is an external traction field exerted on the RVE boundary.

The second assumption, also known as the Hill-Mandel principle, requires that

$$\bar{\boldsymbol{\sigma}} : \bar{\boldsymbol{\varepsilon}} = \frac{1}{V_\mu} \int_{\Omega_\mu} \boldsymbol{\sigma}_\mu : \boldsymbol{\varepsilon}_\mu dV \tag{7}$$

must hold for any kinematically admissible microscopic strain field, $\boldsymbol{\varepsilon}_\mu$.

Accordingly, the macroscopic stress tensor, $\bar{\boldsymbol{\sigma}}$, is taken as the volume average of the microscopic stress field, $\boldsymbol{\sigma}_\mu$, over the RVE:

$$\bar{\boldsymbol{\sigma}}(\mathbf{x}) \equiv \frac{1}{V_\mu} \int_{\Omega_\mu} \boldsymbol{\sigma}_\mu(\mathbf{y}) dV = \frac{1}{V_\mu} \int_{\partial\Omega_\mu} \mathbf{t}^e \otimes \mathbf{y} dA \tag{8}$$

By combining Eq.(6) with Eq.(7) and taking Eq.(2) and (8) into account, we can establish that Eq.(7) is equivalent to the following variational equation:

$$\int_{\partial\Omega_\mu} \mathbf{t}^e \cdot \boldsymbol{\eta} dA = 0 \quad \forall \boldsymbol{\eta} \in \mathscr{V}_\mu \tag{9}$$

As a consequence of Eq.(9), the RVE equilibrium problem is to find, for a given macroscopic strain $\boldsymbol{\varepsilon}$, a displacement fluctuation $\tilde{\boldsymbol{u}}_\mu$ such that

$$\int_{\Omega_\mu} \boldsymbol{\sigma}_\mu(\mathbf{y}) : \nabla_y^s \boldsymbol{\eta} dV = 0 \quad \forall \boldsymbol{\eta} \in \mathscr{V}_\mu \tag{10}$$

subjected to boundary conditions of Eq.(5) and Eq.(9).

In this work, we consider that the constituents of the composite are linear elastic materials. Therefore, we have

$$\sigma_\mu(\mathbf{y}) = \mathbb{C}_\mu \left(\bar{\boldsymbol{\varepsilon}} + \nabla_y^s \tilde{u}_\mu \right). \tag{11}$$

with $\mathbb{C}_\mu$ denoting the microscale material constitutive law. Under this consideration, the RVE equilibrium problem in Eq.(10) is equivalent to solving the following linear variational equation for the field $\tilde{\mathbf{u}}_\mu \in \mathscr{V}_\mu$ under a given

$\boldsymbol{\varepsilon}$,

$$\int_{\Omega_\mu} \nabla_y^s \eta : \mathbb{C}_\mu : \nabla_y^s \tilde{\mathbf{u}}_\mu dV = -\left[\int_{\Omega_\mu} \nabla_y^s \eta : \mathbb{C}_\mu dV\right] : \bar{\boldsymbol{\varepsilon}} \quad \forall \eta \in \mathscr{V}_\mu \tag{12}$$

3. Stochastic finite element implementation

3.1. Boundary conditions in matrix form

The application of appropriate boundary conditions is a key feature in the solution of the RVE boundary value problem. In general, there are several ways to apply the boundary constraints, but three of them are commonly considered in the literature and will be considered in the present study; (1) linear displacement that assumes the displacement field on the boundary of the RVE satisfies $\mathbf{u}_\mu = \bar{\boldsymbol{\varepsilon}}\mathbf{y}$ with $\tilde{\mathbf{u}}_\mu = \mathbf{0}$; (2) periodic boundary condition that assumes the displacement fluctuations on the boundary of RVE are periodic, $\tilde{\mathbf{u}}_+^e = \tilde{\mathbf{u}}_-^e$ while the tractions are anti-periodic, $\mathbf{t}_+^e = -\mathbf{t}_-^e$; (3) uniform traction boundary condition that requires the kinematic constraint on the RVE is minimal and the tractions on the surface of the RVE are prescribed in terms of the macroscopic stress as $\mathbf{t}^e = \bar{\boldsymbol{\sigma}} \cdot \mathbf{n}$ with $\mathbf{n}$ the outward normal at the boundary surface. To impose these three types of boundary condition, the generalized RVE boundary condition enforcement approach proposed by Kaczmarczyk et al. (2008) was adopted with extension to 3D finite element method (FEM) implementation. Accordingly, Eq.(5) is already satisfied with the choice of linear displacement, periodic displacement and anti-periodic traction, and the constant traction boundary condition, and the task is to impose Eq.(9), which is restated in terms of the microscopic

displacement field and the macroscopic strain as

$$\int_{\partial\Omega_\mu} \mathbf{t}^e \cdot (\mathbf{u}_\mu - \bar{\boldsymbol{\varepsilon}}\mathbf{y})\, dA = \mathbf{0} \tag{13}$$

and written in matrix form as

$$\mathbf{Pu} = \mathbf{D}\bar{\boldsymbol{\varepsilon}} = \mathbf{g} \tag{14}$$

where constraint matrix $\mathbf{P}$ and global coordinate matrix $\mathbf{D}$ are defined by

$$\mathbf{P} = \int_{\partial\Omega} \mathbf{H}\mathbf{N}^T\mathbf{N} dA \quad \mathbf{D} = \int_{\partial\Omega} \mathbf{H}\mathbf{N}^T\mathbf{X} dA \tag{15}$$

where $\mathbf{H}$ is a matrix associated with the type of boundary condition considered (see subsequent definitions), $\mathbf{N}$ is the standard shape function matrix and $\mathbf{X}$ is a position matrix evaluated at the integration points on the RVE boundary $\partial\Omega$

$$\mathbf{X} = \frac{1}{2}\begin{bmatrix} 2x & 0 & 0 & y & z & 0 \\ 0 & 2y & 0 & x & 0 & z \\ 0 & 0 & 2z & 0 & x & y \end{bmatrix} \tag{16}$$

with x, y and z calculated by using the known nodal coordinates and shape functions associated with these nodes as

$$\begin{bmatrix} x_1 & \cdots & x_{ng} \\ y_1 & \cdots & y_{ng} \\ z_1 & \cdots & z_{ng} \end{bmatrix} = \begin{bmatrix} x_1^{nd} & x_2^{nd} & x_3^{nd} \\ y_1^{nd} & y_2^{nd} & y_3^{nd} \\ z_1^{nd} & z_2^{nd} & z_3^{nd} \end{bmatrix} \begin{bmatrix} N_1 & \cdots & N_{ng} \\ N_1 & \cdots & N_{ng} \\ N_1 & \cdots & N_{ng} \end{bmatrix} \tag{17}$$

where ng are the total number of Gauss points used in each triangular element on the boundary to perform numerical integration, and x_i^{nd}, y_i^{nd} and z_i^{nd} are nodal coordinates. The terms $\mathbf{N}$ and $\mathbf{X}$ in Eq.(14) are fixed for a given RVE and the nature of the RVE boundary condition is only reflected in the terms

of the $\mathbf{H}$ matrix, that assigns an admissible distribution of nodal traction forces on the boundary of the RVE.

In the case of linear displacements, the tractions on the boundary are not subjected to any constraint and $\mathbf{H}$ is the identity matrix. Conversely, for the case of periodic boundary conditions, the tractions should be anti-periodic and the $\mathbf{H}$ matrix on opposite faces will be $\mathbf{H}^{+} = -\mathbf{H}^{-}$. For the uniform traction boundary condition, the traction contributed by each point is prescribed as $\mathbf{t} = \bar{\boldsymbol{\sigma}} \cdot \mathbf{n}$, or in a matrix form,

$$[\mathbf{t}_i] = \begin{bmatrix} \sigma_{xx}n_x & 0 & 0 \\ 0 & \sigma_{yy}n_y & 0 \\ 0 & 0 & \sigma_{zz}n_z \\ \sigma_{xy}n_y & \sigma_{xy}n_x & 0 \\ \sigma_{xz}n_z & 0 & \sigma_{xz}n_x \\ 0 & \sigma_{yz}n_z & \sigma_{zy}n_y \end{bmatrix}$$

Thus, as an example, $\mathbf{H}$ for a linear triangular element on the negative x-face ($\mathbf{n} = [n_x, n_y, n_z] = [-1, 0, 0]$) is

$$\mathbf{H}_x = \begin{bmatrix} -1 & 0 & 0 & -1 & 0 & 0 & -1 & 0 & 0 \\ 0 & 0 & 0 & 0 & 0 & 0 & 0 & 0 & 0 \\ 0 & 0 & 0 & 0 & 0 & 0 & 0 & 0 & 0 \\ 0 & -1 & 0 & 0 & -1 & 0 & 0 & -1 & 0 \\ 0 & 0 & -1 & 0 & 0 & -1 & 0 & 0 & -1 \\ 0 & 0 & 0 & 0 & 0 & 0 & 0 & 0 & 0 \end{bmatrix} \tag{18}$$

The same procedure is applied to obtain the subset of $\mathbf{H}$ for other surfaces.

3.2. Enforcement of the RVE boundary conditions

We now focus on the finite element solution of the RVE boundary value problem. Following standard notation, the finite element solution to the RVE boundary value problem converts to a constrained quadratic programming problem:

$$\min_{\mathbf{u}} \left\{ \frac{1}{2}\mathbf{u}^T\mathbf{K}\mathbf{u} - \mathbf{u}^T\mathbf{F} \right\} \quad \text{subject to} \quad \mathbf{P}\mathbf{u} - \mathbf{D}\bar{\boldsymbol{\varepsilon}} = \mathbf{0} \tag{19}$$

where $\mathbf{K}$ is the stiffness matrix, $\mathbf{F}$ is the load vector, $\mathbf{P}$ and $\mathbf{D}$ are the previously defined constraint matrix and coordinate matrix respectively. A common method to solve this problem is to introduce Lagrange multipliers $\boldsymbol{\lambda}$ associated with the constraint. The Lagrangian is thus

$$\mathcal{L} = \frac{1}{2}\mathbf{u}^T\mathbf{K}\mathbf{u} - \mathbf{u}^T\mathbf{F} + \boldsymbol{\lambda}^T(\mathbf{P}\mathbf{u} - \mathbf{D}\bar{\boldsymbol{\varepsilon}}) \tag{20}$$

for which the Euler conditions for a stationary point are expressed in matrix form as

$$\begin{bmatrix} \mathbf{K} & \mathbf{P}^T \\ \mathbf{P} & \mathbf{0} \end{bmatrix} \begin{Bmatrix} \mathbf{u} \\ \boldsymbol{\lambda} \end{Bmatrix} = \begin{Bmatrix} \mathbf{F} \\ \mathbf{D}\bar{\boldsymbol{\varepsilon}} \end{Bmatrix} \tag{21}$$

which can then be written in a compact form for convenience as

$$\left[\hat{\mathbf{K}}\right] \{\hat{\mathbf{u}}\} = \left\{\hat{\mathbf{F}}\right\}. \tag{22}$$

Note that, in the absence of body forces, $\mathbf{F} = \mathbf{0}$

3.3. Stochastic finite element formulation

Now consider randomness in the material properties of the constituents and define $\mathbf{b} = \{b_1, b_2, \cdots, b_n\}^T$ as an n-dimensional random vector, that, in the present case, comprises Young's modulus, Poisson's ratio, and shear

modulus. In Eq.(21) or (22), the stiffness matrix $\mathbf{K}$, being a function of the material properties, is thus a stochastic function. The structural response, in terms of displacement $\mathbf{u}$ and Lagrange multipliers $\boldsymbol{\lambda}$, is a stochastic function of the material properties.

Using the perturbation technique (Kleiber and Hien, 1992; Kamiński, 2013), an arbitrary stochastic function, $\varphi(\mathbf{b})$, can be approximated via a second-order Taylor series expansion as:

$$\varphi(\mathbf{b}) = \varphi(\bar{\mathbf{b}}) + \epsilon \sum_{i=1}^{n} \left[D_{b_i}\varphi(\bar{\mathbf{b}})\right] \delta b_i + \epsilon^2 \frac{1}{2} \sum_{i=1}^{n}\sum_{j=1}^{n} \left[H_{b_i b_j}\varphi(\bar{\mathbf{b}})\right] \delta b_i \delta b_j \tag{23}$$

where $\bar{\mathbf{b}}$ is the mean value of the random vector $\mathbf{b}$, δb_i denotes the variation around mean value of the ith random variable, $[D_{b_i}(\varphi)]$ and $\left[H_{b_i b_j}(\varphi)\right]$ denote the first- and second-order partial derivatives of $(\cdot)$ with respect to b_i, and ϵ is a scalar representing a given small perturbation.

By extending the stochastic functions $\hat{\mathbf{F}}$ and $\hat{\mathbf{u}}$ in Eq.(22) to the forms of Eq.(23), substituting into Eq.(22), and equating terms of equal orders of ϵ, we arrive at the following zeroth-, first- and second-order equations:

- The zeroth-order

$$\left[\hat{\mathbf{K}}\right]\{\hat{\mathbf{u}}\} = \left\{\hat{\mathbf{F}}\right\} \tag{24}$$

- The first-oder

$$\sum_{p=1}^{n} \left\{ \left[\hat{\mathbf{K}}\right]\{D_{b_p}\hat{\mathbf{u}}\} + \left[D_{b_p}\hat{\mathbf{K}}\right]\{\hat{\mathbf{u}}\} \right\} = \mathbf{0} \tag{25}$$

- The second-order

$$\sum_{p=1}^{n}\sum_{q=1}^{n} \left\{ \left[\hat{\mathbf{K}}\right]\{H_{b_p b_q}\hat{\mathbf{u}}\} + \left[D_{b_p}\hat{\mathbf{K}}\right]\{D_{b_p}\hat{\mathbf{u}}\} + \left[H_{b_p b_q}\hat{\mathbf{K}}\right]\{\hat{\mathbf{u}}\} \right\} = \mathbf{0} \tag{26}$$

In the present study, we consider material properties as random variables. The block related to stiffness matrix, $[\mathbf{K}]$, of the microstructure in the compact matrix, $\left[\hat{\mathbf{K}}\right]$, is function of material properties. It can be expressed as

$$\mathbf{K} = \int_{\Omega_\mu^s} \mathbf{B}^T \mathbb{C}_\mu \mathbf{B} dV, \tag{27}$$

and its first- and second-order partial derivatives are

$$\left[D_{b_p}\mathbf{K}\right] = \int_{\Omega_\mu^s} \mathbf{B}^T \left[D_{b_p}\mathbb{C}_\mu\right] \mathbf{B} dV, \quad \text{and} \quad \left[H_{b_p b_q}\mathbf{K}\right] = \int_{\Omega_\mu^s} \mathbf{B}^T \left[H_{b_p b_q}\mathbb{C}_\mu\right] \mathbf{B} dV. \tag{28}$$

where $\mathbf{B}$ is the strain-displacement matrix, and $D_{b_p}\mathbb{C}_\mu$ and $H_{b_p b_q}\mathbb{C}_\mu$ are the first- and second-order partial derivatives of the material constitutive matrix. Hence, the expression of $\left[\hat{\mathbf{K}}\right]$ and its first- and second-order partial derivatives can be written as:

$$\left[\hat{\mathbf{K}}\right] = \begin{bmatrix} \mathbf{K} & \mathbf{P}^T \\ \mathbf{P} & \mathbf{0} \end{bmatrix}, \quad \left[D_{b_p}\hat{\mathbf{K}}\right] = \begin{bmatrix} D_{b_p}\mathbf{K} & \mathbf{0} \\ \mathbf{0} & \mathbf{0} \end{bmatrix}, \quad \text{and} \quad \left[H_{b_p b_q}\hat{\mathbf{K}}\right] = \begin{bmatrix} H_{b_p b_q}\mathbf{K} & \mathbf{0} \\ \mathbf{0} & \mathbf{0} \end{bmatrix}. \tag{29}$$

Computing Eqs.(24 - 26) successively, the zeroth order compact displacement vector $\{\hat{\mathbf{u}}\}$ can be derived from Eq.(24). With this at hand, the first order partial derivative of the compact displacement vector $\{\hat{\mathbf{u}}\}$ with respect to the material properties $\mathbf{b}$, i.e. $\left\{D_{b_p}\hat{\mathbf{u}}\right\}$, is determined from Eq.(25). Note that Eq.(25) is solved for each component of $\left\{D_{b_p}\hat{\mathbf{u}}\right\}$ independently. Finally, Eq.(26) is solved to determine the second order partial derivative of the compact displacement vector $\left\{H_{b_p b_q}\hat{\mathbf{u}}\right\}$, once again solving for each term independently.

3.4. Fibre yarn/tow direction computation through potential flow theory

To assemble the global stiffness matrix $\mathbf{K}$, the complex structure of fabric reinforcement of the textile composite causes some difficulty to introduce its contribution when transforming from the material principal coordinate system to the global coordinate system. Commonly, the yarn directions can be calculated from the yarn path, which is normally known to establish geometry modelling. However, it is not robust enough to use for deformed yarns with varying cross-sections. In MoFEM (Kaczmarczyk et. al., 2014), an automated approach based on potential flow theory is used to identify the yarn direction. The principle is to treat each yarn as a invicid, incompressible and irrotational flow with the same the boundary surface as the yarn. In fluid dynamics, the flow can be described by a velocity potential function, ϕ. The velocity field of the flow is the gradient of ϕ with components in Cartesian coordinate expressed as:

$$v_x = \frac{\partial \phi}{\partial x}, \quad v_y = \frac{\partial \phi}{\partial y}, \quad \text{and} \quad v_z = \frac{\partial \phi}{\partial z} \tag{30}$$

For incompressible flow, the velocity potential function satisfies Laplace's function, substituting in the relationship between potential and velocity we arrive at,

$$\nabla^2 \phi = \frac{\partial^2 \phi}{\partial x^2} + \frac{\partial^2 \phi}{\partial y^2} + \frac{\partial^2 \phi}{\partial z^2} = 0 \tag{31}$$

Solving Eq.(31) determine the velocity of the flow that represents the yarn direction for our case. To transform the material response between local yarn direction and global axes, the axis of rotation is expressed as $\mathbf{J} = \mathbf{v} \times \mathbf{e}_i$, where $\mathbf{e}_i$ is the unit vector representing the global x-, y- or z-axis, and the

angle of rotation is calculated by

$$\mathbf{\Theta}(\theta,\psi,\varphi) = \cos^{-1}\left(\frac{\mathbf{ve}_i}{\parallel \mathbf{v} \parallel}\right) \quad i = 1,2,3. \tag{32}$$

With the rotation angle $\mathbf{\Theta}$ and axis of rotation $\mathbf{J}$ at hand, the rotation matrix $\mathbf{R}$, which relates original coordinate system to transformed coordinate $\mathbf{x}^{'} = \mathbf{Tx}$ (see Fig.2), can be obtained according the orthogonal transformation criteria (Filleppa and Haugen, 2005). Then the stress tensor transformation matrix $\mathbf{T}_\sigma$ and strain tensor transformation matrix $\mathbf{T}_\varepsilon$ can be established by the relationship between original coordinate system and transformed coordinate system, and therefore the transformed stiffness matrix transformation matrix,$\hat{\mathbb{C}}$, can be calculated $\hat{\mathbb{C}} = \mathbf{T}_\sigma \mathbb{C} \mathbf{T}_\varepsilon^{-1}$ (Slawinski, 2010).

4. Statistics of the effective elasticity tensor

The objective of a homogenization procedure is to determine the effective elastic moduli, $\bar{\mathbb{C}}$. In the computational homogenization approach no explicit form of the constitutive behaviour on the the macrolevel is assumed a priori, so that the tangent modulus has to be determined numerically by the relations between the macroscopic stress, $\bar{\boldsymbol{\sigma}}$, and the macroscopic strain, $\bar{\boldsymbol{\varepsilon}}$.

Given that the solutions from Eq. (21) or (22) for $\mathbf{u}$ and $\boldsymbol{\lambda}$ satisfies the equilibrium, the work done by the tractions on the displacements is equal to the work of the generalized tractions on the generalized displacements:

$$\mathbf{u}^T \mathbf{t} = \left(\mathbf{D}\bar{\boldsymbol{\varepsilon}}\right)^T \boldsymbol{\lambda} \tag{33}$$

With reference to Eq. (8), the macrostress vector can be expressed in terms

of the Lagrange multipliers $\boldsymbol{\lambda}$ and matrix $\mathbf{D}$:

$$\bar{\boldsymbol{\sigma}} = \frac{1}{V_\mu}\mathbf{D}^T\boldsymbol{\lambda} \tag{34}$$

Straightforwardly, the effective moduli can be computed in its discretised form, using previous averaged stress expression Eq. (34), in the following way:

$$\bar{\mathbb{C}} = \frac{\bar{\boldsymbol{\sigma}}}{\bar{\boldsymbol{\varepsilon}}} = \frac{1}{V_\mu}\frac{\mathbf{D}^T\boldsymbol{\lambda}}{\bar{\boldsymbol{\varepsilon}}} \tag{35}$$

In practice, it follows from the above equation that the effective material stiffness, $\bar{\mathbb{C}}$, can be determined efficiently by first factorising $\hat{\mathbf{K}}$ and then solving Eq.(22) six times for every strain mode, with $\bar{\boldsymbol{\varepsilon}}$ a unit vector.

4.1. Stochastic expression of effective elastic moduli

Since the micro-structure displacement $\mathbf{u}$ is function of material properties, and the effective elastic tensor, $\bar{\mathbb{C}}$, is thus a stochastic function when considering material properties as random variables. It can be approximated by the perturbation technique using a second-order Taylor series expansion, as,

$$\left[\bar{\mathbb{C}}(\mathbf{b})\right] = \left[\bar{\mathbb{C}}(\bar{\mathbf{b}})\right] + \epsilon\sum_{r}^{n}\left[D_{b_r}\bar{\mathbb{C}}(\bar{\mathbf{b}})\right]\delta b_r + \epsilon^2\frac{1}{2}\sum_{r}^{n}\sum_{s}^{n}\left[H_{b_r b_s}\bar{\mathbb{C}}(\bar{\mathbf{b}})\right]\delta b_r \delta b_s \tag{36}$$

where the first- and second-order partial derivative terms $\left[D_{b_r}\bar{\mathbb{C}}(\bar{\mathbf{b}})\right]$ and $\left[H_{b_r b_s}\bar{\mathbb{C}}(\bar{\mathbf{b}})\right]$ can be calculated by using Eqs.(25, 26, 35).

4.2. Mean and covariance

Given the approximation for $\bar{\mathbb{C}}(\mathbf{b})$ in Eq.(36), the mean value of the elasticity moduli is expressed as

$$\begin{aligned} E\left[\bar{\mathbb{C}}(\mathbf{b})\right] &= \int_{-\infty}^{+\infty} \bar{\mathbb{C}}(\mathbf{b}) g(\mathbf{b}) d\mathbf{b} \\ &= \int_{-\infty}^{+\infty} \left\{ \left[\bar{\mathbb{C}}(\bar{\mathbf{b}})\right] + \epsilon \sum_r \left[D_{b_r} \bar{\mathbb{C}}(\bar{\mathbf{b}})\right] \delta b_r \right. \\ &\quad \left. + \epsilon^2 \frac{1}{2} \sum_r \sum_s \left[H_{b_r b_s} \bar{\mathbb{C}}(\bar{\mathbf{b}})\right] \delta b_r \delta b_s \right\} g(\mathbf{b}) d\mathbf{b} \end{aligned} \tag{37}$$

where $g(\mathbf{b})$ is the probability distribution function, that is assumed in this paper to be Gaussian. Furthermore, the covariance is expressed as

$$\begin{aligned} \mathrm{Cov}\left(\left[\bar{\mathbb{C}}(\mathbf{b})\right]_r, \left[\bar{\mathbb{C}}(\mathbf{b})\right]_s\right) = \int_{-\infty}^{+\infty} &\left\{\left[\bar{\mathbb{C}}(\mathbf{b})\right]_r - E\left[\bar{\mathbb{C}}(\mathbf{b})\right]\right\} \\ &\times \left\{\left[\bar{\mathbb{C}}(\mathbf{b})\right]_s - E\left[\bar{\mathbb{C}}(\mathbf{b})\right]\right\} g(\mathbf{b}) d\mathbf{b} \end{aligned} \tag{38}$$

Observing the following

$$\int_{-\infty}^{+\infty} g(\mathbf{b}) d\mathbf{b} = 1, \quad \int_{-\infty}^{+\infty} \delta\mathbf{b} g(\mathbf{b}) d\mathbf{b} = 0, \quad \text{and} \quad \int_{-\infty}^{+\infty} \delta\mathbf{b}_r \delta\mathbf{b}_s g(\mathbf{b}) d\mathbf{b} = \mathrm{COV}(b_r, b_s) \tag{39}$$

the second-order approximation of the mean value and covariance for the reduced stiffness matrix is thus calculated as:

$$E\left[\bar{\mathbb{C}}(\mathbf{b})\right] = \left[\bar{\mathbb{C}}(\bar{\mathbf{b}})\right] + \frac{1}{2} \sum_r^n \sum_s^n \left[H_{b_r b_s} \bar{\mathbb{C}}(\bar{\mathbf{b}})\right] \cdot \mathrm{COV}(b_r, b_s), \tag{40}$$

and

$$\begin{aligned} \mathrm{COV}\left(\left[\bar{\mathbb{C}}(\mathbf{b})\right]_r, [\mathbb{C}(\mathbf{b})]_s\right) \approx &\sum_r^n \sum_s^n \left[D_{b_r} \bar{\mathbb{C}}(\bar{\mathbf{b}})\right] \left[D_{b_s} \bar{\mathbb{C}}(\bar{\mathbf{b}})\right] \cdot \mathrm{COV}(b_r, b_s) \\ &+ \frac{1}{4} \sum_r^n \sum_s^n \sum_t^n \sum_w^n \left[H_{b_r b_s} \bar{\mathbb{C}}(\bar{\mathbf{b}})\right] \left[H_{b_t b_w} \bar{\mathbb{C}}(\bar{\mathbf{b}})\right] E\left[b_r b_s b_t b_w\right]. \end{aligned} \tag{41}$$

5. Numerical example

The analysis of two plain weave textile composites is used to demonstrate the method described in the preceding sections. The effective elastic properties and their statistics are predicted. The accuracy of the proposed method is evaluated by comparing the statistics of effective elastic properties against corresponding values obtained using a Monte Carlo simulation (MCS) method. Relations between the variations of input variables and statistics of the effective elastic properties are also investigated in terms of sensitivity analyses.

5.1. Geometric modelling and meshing of RVE microstructure

Two RVE microstructures with plain weave fabric reinforcement (Barbero et al., 2005) and (Scida et al., 1999) are selected to evaluate the applicability of computational homogenization scheme for textile composites, comparing with experimental and/or existing model results. These two models are named the Barbero model and the Scida model here after. The Barbero model is based on photomicrograph measurements of geometrical parameters and the Mori-Tanaka asymptotic homogenization method has been applied to predict the effective elastic parameters (Barbero et al., 2005). The geometrical parameters of the Scida model was also obtained by photomicrography, and experiments were conducted to obtain the longitudinal and transversal Young's moduli and the in-plane Poisson's ratio. An analytical model was developed, based on classic thin laminate theory, to estimate the effective elastic properties (Scida et al., 1999). Both models are characterized by the same idealized periodic microstructure model proposed by Barbero et al.

(2005), with the yarns' cross-sections and the path of the yarns taking the form of the sinusoidal functions $F(x,y) = A(x) \cdot sin(B(x) \cdot y + C(x)) + D(x)$ and $F(x,y) = A(y) \cdot sin(B(y) \cdot x + C(y)) + D(y)$, with coefficients A, B, C and D determined from the geometric parameters. The geometry of the plain weave composite is shown in Fig. 3 and comprises four interlaced fibre yarns. It is described through the periodic length of warp and weft yarns, $4a_1$ and $4a_2$, respectively, waviness amplitude $2a_3$, and spacing between adjacent warp or weft yarns, a_{g1} and a_{g2}. Therefore, the dimension of the RVE is $4a_1 \times 4a_2 \times 2a_3$. These parameters are illustrated in Fig. 3 and their values are listed in Table 1. The RVE consists of an isotropic epoxy matrix and carbon fibre yarns that are assumed to be transversely isotropic material. The warp and weft yarns are made of identical material. Although the volume of the yarn is not entirely occupied by fibres due to the flow of epoxy through the fibrous preform during infusion, the yarn is considered as a solid volume in this work in order to focus our attention on material properties. A total of seven independent material parameters are used to describe the matrix and yarn and their values are presented in Table 2.

With geometrical parameters and the mathematical formulation for the idealized periodic microstructure model available, the 3D geometric models of Barbero model and Scida model are created using CUBIT, which is a software toolkit for two- and three-dimensional finite element meshes and geometry preparation developed by Sandia National Laboratories in the United States of America. The cross-section curves and the yarn path curves describing the warp and weft yarns are constructed with the sinusoidal function model proposed by Barbero et al. (2005) and geometric parameters listed in Table

1. A solid volume can be created by sweeping the cross section surfaces along the path curves. Hence, four interlaced yarn volumes are generated with two of them for warp and the other two for weft. Although the mathematical model provides a perfect common surface between interlaced warp and weft yarns, overlapping has been found that is unrealistic and results in meshing errors. To avoid the overlapping problem, a small gap is introduced between weft and warp yarns by slightly increasing the waviness amplitude a_3 for yarn path curves but keeping the a_3 unchanged when creating cross section curves.

The generated 3D geometric models are then discretized using 4 node tetrahedral elements and the mesh operation in CUBIT. Given the need for periodic boundary conditions for the computational homogenization, the resulting mesh should be perfectly symmetrical between opposite boundary surfaces. For instance, the meshes on the $+x$ surface should match with those on the $-x$ surface. Hence, the positive boundary surfaces, $+x$, $+y$ and $+z$ are meshed first with triangular element and then the meshes are copied to the corresponding negative boundary surfaces $-x$, $-y$ and $-z$. The RVE is then finally meshed into tetrahedral elements based on these meshed surfaces. The RVE of the Barbero model has been discretized into 12148 four-node tetrahedral elements consisting of 5346 elements for the yarns and 6802 elements for the matrix, with a total of 2454 nodes, while the RVE of Scida model has been discretized into 20053 tetrahedral elements with 8101 of them for the yarns and 11952 for matrix.

5.2. *Application of the computational homogenization for woven textile composites*

The meshed models of the RVEs are imported into the MoFEM finite element programme. As previously noted, the wavy yarns leads difficulty to introduce their contributions to assemble global stiffness matrix when transforming from the material principal coordinate system to the global coordinate system, especially for transisotropic materials such as carbon fibre, and the potential flow theory approach is adopted in the present study to automatically identify yarn directions. A potential flow calculation is thus run first for the fabric reinforcement. Constant pressure is applied to each yarns as shown in Fig. 4a, and the flow velocity can be calculated from Eq.(31). Using these calculated flow velocities (see Fig. 4b), the yarn directions can be calculated from Eq.(32). With the obtained direction of yarn elements, RVE homogenization calculation is ready to be conducted on MoFEM.

Before considering stochastic analysis, first the applicability of the computational homogenization method for textile composite is demonstrated. Two verification studies are performed. The first study is designed to demonstrate that the proposed method can capture the waviness feature of textile composite by comparing results for an RVE reinforced by crimp yarns with those for an RVE reinforced by straight yarns. Three patterns of reinforcement are considered from single yarn to four interlaced yarns, see Fig. 5. Results are listed in Table 3 for an RVE under periodic displacement and anti-periodic traction boundary conditions. The effective engineering properties are recovered from the computationed homogenization method estimated effective moduli in Eq. (35) by using the equations listed in Appendix A. By ob-

serving the results of the estimated $\bar{\mathbb{C}}$, the textile composite is treated as an orthotropic material. For the single yarn case, the longitudinal modulus, E_x, significantly decreases from 24.64 GPa for a straight yarn to 15.35 GPa for a crimped yarn due to the waviness of the yarn. The other terms are almost unchanged. For crossed yarns, the transverse modulus has a significant increase for both the straight and crimp yarns, while the other terms have slight increase. As expected, the stiffness for the crimp yarn structure is smaller than for straight yarns. For the interlaced yarn case, the effective material properties have significantly increase again with the contribution from additional two yarns comparing with the cross case.

In the second verification study, the effective engineering parameters predicted by the adopted computational homogenization method are compared with experimental and/or numerical results. The results are listed in Table 4. The reference numerical results for both models are taken from (Barbero et al., 2005), where both models have been analysed using the Mori-Tanaka asymptotic homogenization method. For the Scida model, the experimental results reported are from (Scida et al., 1999). For the computational homogenization, the results for the three boundary conditions of linear displacement (Disp.), periodic (Per.), and constant traction (Trac.) are given in the table. From these results it can be seen that the model predicts moduli values that are within or very near the published standard deviation.

5.3. Accuracy of the proposed method for uncertainty quantification

To demonstrate the accuracy of the present perturbation-based stochastic multi-scale computational homogenization method, a comparison between the present approach and MCS with 5000 samples has been performed. The

results for the RVE of the Barbero model are also given in details for illustration purposes. Uncertainties in the seven material properties of the composite material were considered separately with coefficient of variation (CV) of 0.1 for each and mean values as listed in Table 2, and the material properties are considered to follow Normal distributions. Results are given in Fig. 6 and Table 5 for the mean value from Eq.(40) and Fig. 7 and Table 6 for the coefficient of variation from Eq.(41). Since the influence of variation of material properties on the mean value will be relatively small (see Eq.(40)), we only show a comparison between the proposed method and MCS for variation in the yarn longitudinal Young's modulus. From these results, it can be seen that the mean values estimated by the proposed approach are in close agreement with those obtained from MCS with relative percentage differences (RPD) of less than 1%. In general, these figures indicate that CV of each component of the effective elastic tensor are accurately estimated by the proposed method. The variation due to the randomness of E_z, ν_p, ν_z, G_z and E_m are well captured.

Nevertheless, it is worth noting that the variability in the components of effective elastic properties, $\mathbb{C}_{12}$, $\mathbb{C}_{13}$, $\mathbb{C}_{22}$, $\mathbb{C}_{23}$ and $\mathbb{C}_{33}$, arising from the uncertainty of ν_m are not well predicted as shown in Table 6. A further study was conducted to explore the potential reasons for this by varying the CV of ν_m from 0.025 to 0.15. The estimated CV of the effective elastic properties from the proposed method have been compared with corresponding results obtained by MCS with 5000 samples in terms of RPD. In general, the RPD becomes larger with increases of CV for ν_m as shown in Fig. 8. The RPDs for $\mathbb{C}_{44}$, $\mathbb{C}_{55}$ and $\mathbb{C}_{66}$ may be considered as acceptable, as less than 5%. For

the remaining terms, $\mathbb{C}_{11}$, $\mathbb{C}_{12}$, $\mathbb{C}_{13}$, $\mathbb{C}_{22}$, $\mathbb{C}_{23}$ and $\mathbb{C}_{33}$, the CV of ν_m must be less than 0.05 to keep the RPD less than 5%. The RPDs are around 30% when ν_m has CoV of 0.15. From a theoretical viewpoint, the effective elastic properties are nonlinear functions of ν_m. For instance, $\mathbb{C}_{11}$ has contribution from the isotropic material phase $\frac{E_m(1-\nu_m)}{(1+\nu_m)(1-2\nu_m)}$, whereas the second-order Taylor series expansion to approximate the stochastic function has a slower rates of convergence compared with the original function, especially when the variation is large. When the ν_m is close to 0.5, it results in division by zero problem in $\frac{E_m(1-\nu_m)}{(1+\nu_m)(1-2\nu_m)}$. For instance, 2, 16, 66 and 149 random numbers in the 5000 samples for CV of 0.075, 0.1, 0.125 and 0.15 cases are greater than 0.45.

5.4. Sensitivity analysis

Another important issue in uncertainty analysis is to understand how the variation in the elastic properties of constituents affect the statistical features of the effective elastic properties. This can be addressed by conducting a sensitivity analysis, which is a by-product of the proposed PSMFE method. Fig. 9 shows how the CV for the material properties of the constituents influence the CV for different components of the effective elastic tensor when using the three different boundary conditions. The CVs of the material properties are assumed to be 0.1 to ensure the estimates of the CVs for the effective elastic properties are satisfactorily predicted as demonstrated in the previous section. The response of the effective elastic properties varies with different material properties. From Fig. 9 some observations can be drawn: (1) Under different boundary conditions, the key features of the variation for the effective elastic properties are similar; (2) The variation of $\mathbb{C}_{11}$ and

$\mathbb{C}_{22}$ is most sensitive to the variation of E_z; (3) The variation of $\mathbb{C}_{12}$, $\mathbb{C}_{13}$ and $\mathbb{C}_{23}$ are correlated with almost all material properties except for G_z, and they are significantly dependent on the variation of the material properties of the matrix; (4) The variations of E_m and ν_m of the matrix have significant influence on the variation of $\mathbb{C}_{33}$; (5) The variation of components $\mathbb{C}_{55}$ and $\mathbb{C}_{66}$ mainly depend on the variation of E_m. Variation of G_z is the main source of uncertainty for $\mathbb{C}_{66}$.

5.5. P-refinement of the RVE finite element mesh

P-refinement of the RVE finite element mesh is achieved by using the strategy proposed by Ainsworth and Coyle (2003) for tetrahedral elements with hierarchic approximations. As shown in Fig. 10, a tetrahedral element can be described by 4 vertices ($v_i, i = 1, \cdots, 4$), 6 edges ($e_j, j = 1, \cdots, 6$), 4 triangular faces ($f_k, k = 1, \cdots, 4$) and an interior tetrahedral body. The degrees of freedom for each sub-element depend on the order of polynomial function of the shape function as given in Fig. 10. The total degrees of freedom is then obtained from the sum of the subelements. Thus, it is possible to increase the level of approximation without changing the original finite element mesh. To illustrate the efficacy of p-refinement, a coarse mesh with 6747 elements and a fine mesh with 12093 elements are considered with polynomial orders of approximation $p = 1, 2, 3$ was carried out. Results of the statistics of the effective elastic properties for the two meshes are shown in Fig. 11. We can observe that the mean value (see Fig. 11a) significantly changes when increasing polynomial degree from $p = 1$ to $p = 2$, especially for the coarse mesh. As expected, the mean value tends to converge to a "true value" with increasing polynomial order, which can be observed from Figs.

11a and 11b, with the polynomial order increasing from $p = 2$ to $p = 3$.

6. Conclusions

In this paper, a probabilistic homogenization method is proposed for the prediction of the effective elastic properties of textile composites when taking randomness of the elastic properties of the constituents into consideration. A state-of-the-art computational homogenization scheme, which introduces a hierarchy of boundary conditions at the microscale and allows for direct treatment of micro-to-macro transitions, is adopted as the basis to develop the probabilistic homogenization method. Accurate modelling the fabric reinforcement plays an important rule in the prediction of the effective elastic properties of textile composites due to their complex structure. The p-version of the finite element method is adopted in the present study to refine the analysis. The second-order perturbation method is adopted to estimate the statistics of the components of the effective elastic tensor with the randomness arising from the material properties at mesoscale. Numerical studies have been conducted to demonstrate the capability of the proposed method in capturing variability in effective elastic properties for composites induced by randomness of the constituents' material properties. Plain-weave textile composites consisting of epoxy matrix and carbon fibre yarn have been considered. A comparison with Monte Carlo simulation shows that the proposed probabilistic homogenization method could provide a reasonable prediction for the statistics of the effective material properties.

Acknowledgement

The authors gratefully acknowledge the financial support provided for this study by the UK Engineering and Physical Sciences Research Council (EPSRC) under grant reference EP/K026925/1.

References

Ainsworth, M., Coyle, J., 2003. Hierarchic finite element bases on unstructured tetrahedral meshes. International Journal for Numerical Methods in Engineering 58 (14), 2103–2130.

Barbero, E. J., Damiani, T. M., Trovillion, J., 2005. Micromechanics of fabric reinforced composites with periodic microstructure. International Journal of Solids and Structures 42 (9-10), 2489–2504.

Carvelli, V., Poggi, C., 2001. A homogenization procedure for the numerical analysis of woven fabric composites. Composites Part A: Applied Science and Manufacturing 32 (10), 1425–1432.

Chou, T. W., Ishikawa, T., 1983. One-dimensional micromechanical analysis of woven fabric composites. AIAA Journal 21 (12), 1714–1721.

Clément, A., Soize, C., Yvonnet, J., 2012. Computational nonlinear stochastic homogenization using a nonconcurrent multiscale approach for hyperelastic heterogeneous microstructures analysis. International Journal for Numerical Methods in Engineering 91 (8), 799–824.

Clément, A., Soize, C., Yvonnet, J., 2013. Uncertainty quantification in computational stochastic multiscale analysis of nonlinear elastic materi-

als. Computer Methods in Applied Mechanics and Engineering 254 (0), 61–82.

Fillep, S., Mergheim, J., Steinmann, P., 2013. Computational modelling and homogenization of technical textiles. Engineering Structures 50 (0), 68–73.

Filleppa, C. A., Haugen, B., 2005. A unified formulation of small-strain corotational finite elements: I. theory. Computer Methods in Applied Mechanics and Engineering 194, 2285–2335.

Gager, J., Pettermann, H. E., 2012. Numerical homogenization of textile composites based on shell element discretization. Composites Science and Technology 72 (7), 806–812.

Ghanem, R. G., Spanos, P. D., 2003. Stochastic finite elements: a spectral approach. Civil, Mechanical and Other Engineering Series. Courier Dover Publications.

Gommers, B., Verpoest, I., Van Houtte, P., 1998. The Mori-Tanaka method applied to textile composite materials. Acta Materialia 46 (6), 2223–2235.

Ishikawa, T., Chou, T. W., 1982. Stiffness and strength behaviour of woven fabric composites. Journal of Materials Science 17 (11), 3211–3220.

Ivanov, I., Tabiei, A., 2001. Three-dimensional computational micro-mechanical model for woven fabric composites. Composite Structures 54 (4), 489–496.

Kaczmarczyk, L., Pearce, C. J., Bićanić, N., 2008. Scale transition and enforcement of RVE boundary conditions in second-order computational ho-

mogenization. International Journal for Numerical Methods in Engineering 74 (3), 506–522.

Kaczmarczyk et. al., 2014. Mesh Oriented Finite Element Method (MoFEM), Version 0.1.4. University of Glasgow, Glasgow, UK.
URL https://bitbucket.org/likask/mofem-joseph/wiki/Home/

Kamiński, M., 2007. Generalized perturbation-based stochastic finite element method in elastostatics. Computers & Structures 85 (10), 586–594.

Kamiński, M., 2013. The stochastic perturbation method for computational mechanics. John Wiley & Sons.

Kamiński, M., Kleiber, M., 2000. Perturbation based stochastic finite element method for homogenization of two-phase elastic composites. Computers & Structures 78 (6), 811–826.

Kleiber, M., Hien, T. D., 1992. The stochastic finite element method - Basic perturbation technique and computer implementation. John Wiley & Sons.

Kouznetsova, V., Brekelmans, W. A. M., Baaijens, F. P. T., 2001. An approach to micro-macro modeling of heterogeneous materials. Computational Mechanics 27 (1), 37–48.

Matthies, H. G., 2007. Uncertainty Quantification with Stochastic Finite Elements. John Wiley & Sons, Ltd, book section 27, pp. 1–36.

Michel, J. C., Moulinec, H., Suquet, P., 1999. Effective properties of composite materials with periodic microstructure: a computational approach.

Computer Methods in Applied Mechanics and Engineering 172 (14), 109–143.

Miehe, C., Koch, A., 2002. Computational micro-to-macro transitions of discretized microstructures undergoing small strains. Archive of Applied Mechanics 72 (4-5), 300–317.

Naik, R., 1994. Analysis of woven and braided fabric reinforced composites. Report NASA Contractor Report 194930, Analytical Services & Materials, Inc.

Peng, X., Cao, J., 2002. A dual homogenization and finite element approach for material characterization of textile composites. Composites Part B: Engineering 33 (1), 45–56.

Perić, D., de Souza Neto, E. A., Feijo, R. A., Partovi, M., Molina, A. J. C., 2011. On micro-to-macro transitions for multi-scale analysis of non-linear heterogeneous materials: unified variational basis and finite element implementation. International Journal for Numerical Methods in Engineering 87 (1-5), 149–170.

Sakata, S., Ashida, F., Kojima, T., 2008a. Stochastic homogenization analysis on elastic properties of fiber reinforced composites using the equivalent inclusion method and perturbation method. International Journal of Solids and Structures 45 (2526), 6553–6565.

Sakata, S., Ashida, F., Kojima, T., Zako, M., 2008b. Three-dimensional stochastic analysis using a perturbation-based homogenization method for

elastic properties of composite material considering microscopic uncertainty. International Journal of Solids and Structures 45 (34), 894–907.

Sankar, B. V., Marrey, R. V., 1997. Analytical method for micromechanics of textile composites. Composites Science and Technology 57 (6), 703–713.

Scida, D., Aboura, Z., Benzeggagh, M. L., Bocherens, E., 1999. A micromechanics model for 3D elasticity and failure of woven-fibre composite materials. Composites Science and Technology 59 (4), 505–517.

Slawinski, M. A., 2010. Waves and rays in elastic continua. World Scientific.

Spanos, P. D., Kontsos, A., 2008. A multiscale monte carlo finite element method for determining mechanical properties of polymer nanocomposites. Probabilistic Engineering Mechanics 23 (4), 456–470.

Sriramula, S., Chryssanthopoulos, M. K., 2009. Quantification of uncertainty modelling in stochastic analysis of FRP composites. Composites Part A: Applied Science and Manufacturing 40 (11), 1673–1684.

Stig, F., Hallstrm, S., 2012. A modelling framework for composites containing 3D reinforcement. Composite Structures 94 (9), 2895–2901.

Sudret, B., Der Kiureghian, A., 2000. Stochastic finite element methods and reliability: a state-of-the-art report. Report Technical Report no UCB/SEMM-2000/08, University of California, Berkeley.

Tootkaboni, M., Graham-Brady, L., 2010. A multi-scale spectral stochastic method for homogenization of multi-phase periodic composites with ran-

dom material properties. International Journal for Numerical Methods in Engineering 83 (1), 59–90.

Vandeurzen, P., Ivens, J., Verpoest, I., 1996. A three-dimensional micromechanical analysis of woven-fabric composites: II. elastic analysis. Composites Science and Technology 56 (11), 1317–1327.

List of Tables

Table 1: Geometrical parameters of the woven textile RVE, unit: μm

Term	Symbol	Barbero	Scida
Warp direction	a_1	920	600
Warp yarn spacing	a_{g1}	170	20
Weft direction	a_2	920	600
Weft yarn spacing	a_{g2}	170	20
Waviness amplitude	a_3	250	50
RVE length	l	3680	2400
RVE width	w	3680	2400
RVE thickness	h	500	100

Table 2: Material properties of carbon fibre yarn and epoxy matrix, (moduli in GPa)

Fibre yarn				Matrix			
Property		Barbero	Scida	Property		Barbero	Scida
Axial modulus	E_z	160.755	58.397	Modulus	E_m	3.4	3.4
Transverse modulus	E_p	19.489	20.865	Poisson's ratio	ν_m	0.35	0.35
Axial Poisson's ratio	ν_z	0.28	0.241				
Transverse Poisson's ratio	ν_p	0.415	0.386				
Axial shear modulus	G_z	7.393	8.465				

Table 3: Comparison of the predicted effective elastic properties for composites with straight and crimp yarn (moduli in GPa)

EEP	Single		Cross		Interlace	
	Straight	Crimp	Straight	Crimp	Straight	Crimp
E_x	24.64	15.35	26.85	19.59	50.02	32.17
E_y	5.06	5.04	26.81	19.69	50.02	32.16
E_z	4.67	4.57	6.90	6.53	9.64	9.21
G_{yz}	1.43	1.44	2.09	2.13	2.60	2.69
G_{xz}	1.47	1.52	2.08	2.10	2.60	2.69
G_{xy}	1.67	1.67	2.79	2.78	3.92	4.02
ν_{yz}	0.47	0.45	0.446	0.465	0.426	0.426
ν_{xz}	0.344	0.397	0.446	0.465	0.426	0.426
ν_{xy}	0.332	0.298	0.085	0.100	0.064	0.108

Table 4: Comparison of predicted and reference effective elastic properties (moduli in GPa)

EEP	Barbero model				Scida model				
	Barbero	Comp. homo.			Measured	Barbero	Comp. homo.		
		Disp.	Per.	Trac.			Disp.	Per.	Trac.
E_x	41.106	37.028	32.560	21.051	24.8 ±1.1	24.900	23.060	22.807	20.204
E_y	41.107	37.013	32.565	21.111	24.8 ±1.1	24.900	23.060	22.807	20.210
E_z	9.807	9.725	9.304	7.828	8.5 ±2.6	10.400	9.263	9.002	8.176
G_{yz}	3.077	3.119	2.720	2.435	4.2 ±0.7	2.910	2.750	2.500	2.351
G_{xz}	3.077	3.116	2.720	2.436	4.2 ±0.7	2.910	2.750	2.500	2.351
G_{xy}	3.574	4.417	4.066	3.899	6.5 ±0.8	4.380	5.149	4.784	4.711
ν_{yz}	0.437	0.448	0.426	0.454	0.28±0.07	0.345	0.377	0.373	0.391
ν_{xz}	0.437	0.449	0.426	0.454	0.28±0.07	0.345	0.377	0.373	0.391
ν_{xy}	0.059	0.077	0.107	0.129	0.1 ±0.01	0.130	0.144	0.144	0.160

Table 5: Relative percentage difference on mean value between the proposed method and MCS for different material properties (%)

	$\mathbb{C}_{11}$	$\mathbb{C}_{12}$	$\mathbb{C}_{13}$	$\mathbb{C}_{22}$	$\mathbb{C}_{23}$	$\mathbb{C}_{33}$	$\mathbb{C}_{44}$	$\mathbb{C}_{55}$	$\mathbb{C}_{66}$
E_m	-0.0374	-0.0586	-0.1161	-0.0373	-0.1160	-0.1098	-0.0396	-0.1137	-0.1157
ν_m	0.0638	0.3496	0.4754	0.0641	0.4751	0.2689	0.0117	0.0359	0.0359
ν_p	-0.0124	-0.0567	-0.0632	-0.0124	-0.0632	-0.0192	0.0011	0.0055	0.0055
ν_z	-0.0125	-0.0685	-0.0322	-0.0125	-0.0322	-0.0027	-8.27e-5	-2.04e-4	-2.07e-4
E_p	-0.0290	0.0048	-0.0270	-0.0290	-0.0270	-0.0558	-0.0053	-0.0300	-0.0300
E_z	-0.0901	-0.0885	-0.0386	-0.0902	-0.0385	-0.0023	-6.53e-4	-0.0075	-0.0075
G_z	-0.0344	-0.0445	0.0041	-0.0344	0.0041	-0.0011	-0.1166	-0.0199	-0.0198

Table 6: Relative percentage difference on CV between the proposed method and MCS for different material properties (%)

	$\mathbb{C}_{11}$	$\mathbb{C}_{12}$	$\mathbb{C}_{13}$	$\mathbb{C}_{22}$	$\mathbb{C}_{23}$	$\mathbb{C}_{33}$	$\mathbb{C}_{44}$	$\mathbb{C}_{55}$	$\mathbb{C}_{66}$
E_m	1.4722	1.1155	1.3365	1.4700	1.3364	1.3802	1.4696	1.3529	1.3520
ν_m	24.6721	22.0496	21.7768	24.7736	21.7868	21.3662	-0.3313	-0.8463	-0.8569
ν_p	1.6609	1.5563	1.6135	1.6645	1.6147	1.7624	0.9049	1.0152	1.0136
ν_z	1.2531	1.2417	1.2118	1.2530	1.2118	1.2541	1.3176	0.8308	0.8283
E_p	1.1047	1.1006	2.1484	1.1049	2.1420	1.8045	2.2628	2.2603	2.2602
E_z	1.4243	1.2469	1.4080	1.4243	1.4064	1.4918	1.6464	1.4728	1.4504
G_z	1.5052	1.0548	1.6399	1.5052	1.6386	1.9713	1.2579	1.9432	1.9420

List of Figures

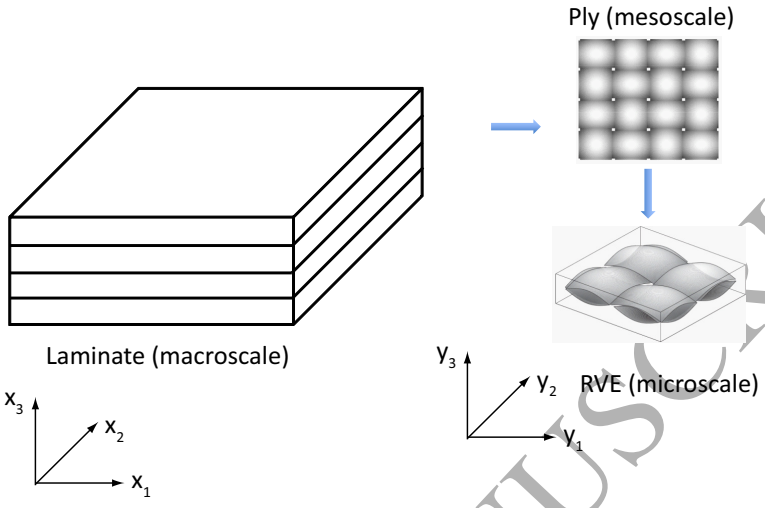

Figure 1: Schematic illustration of the composite volume

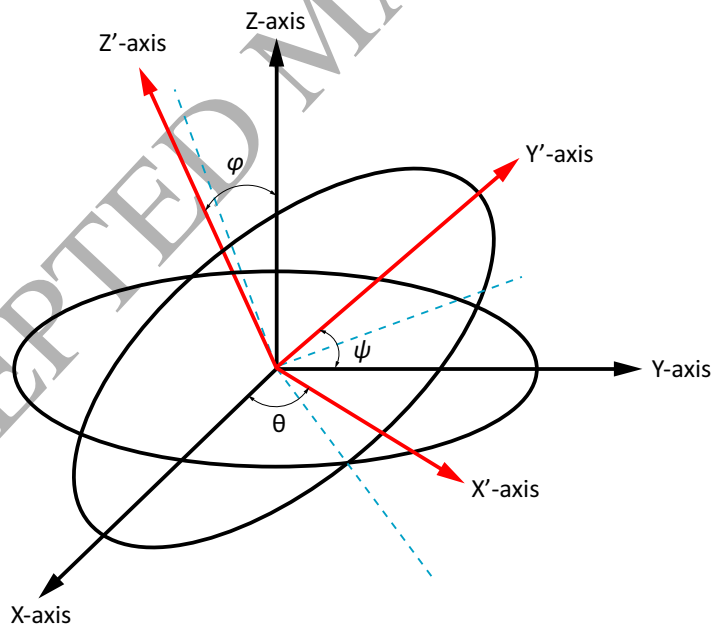

Figure 2: Three dimensional rotation

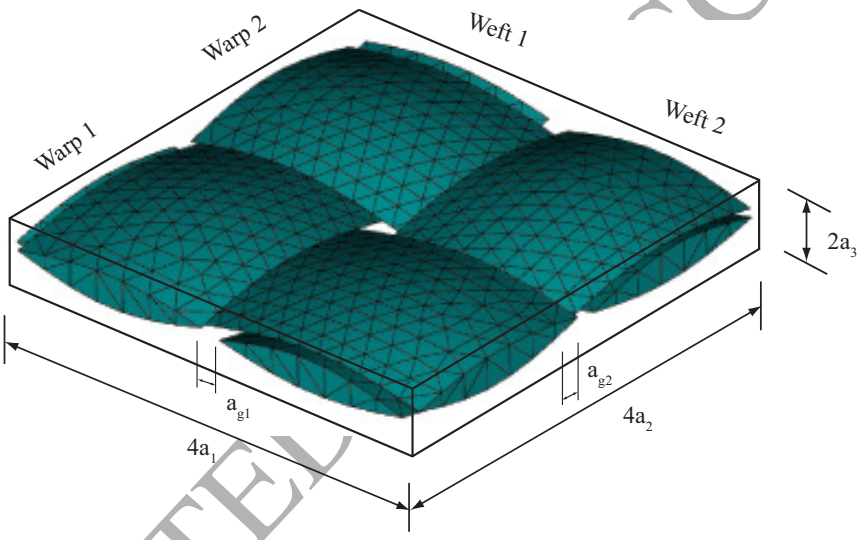

Figure 3: Geometry of the RVE and the finite element mesh of the reinforcement

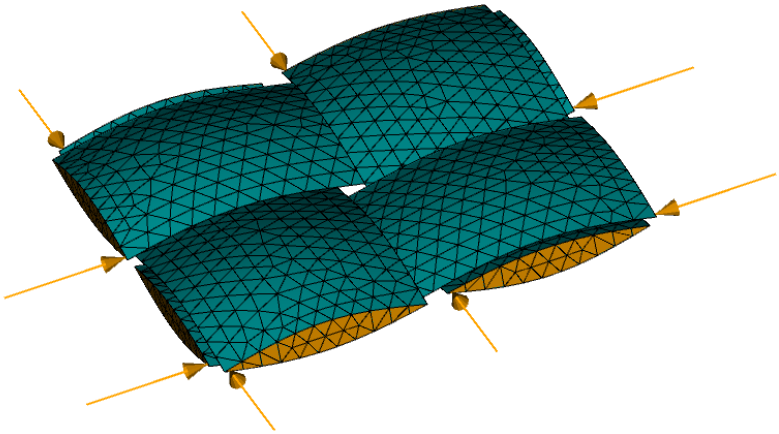

(a) Applying constant pressure to each yarn

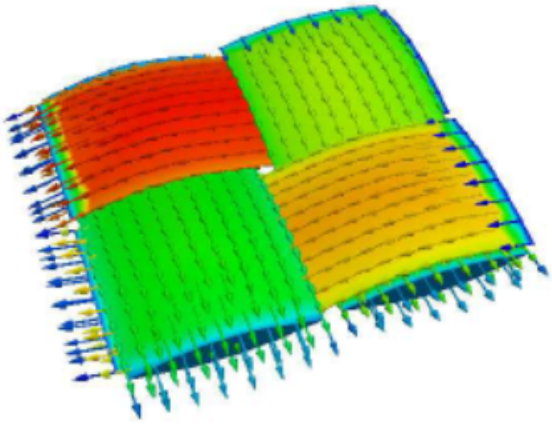

(b) Potential flow

Figure 4: Fibre direction - calculated through potential flow theory

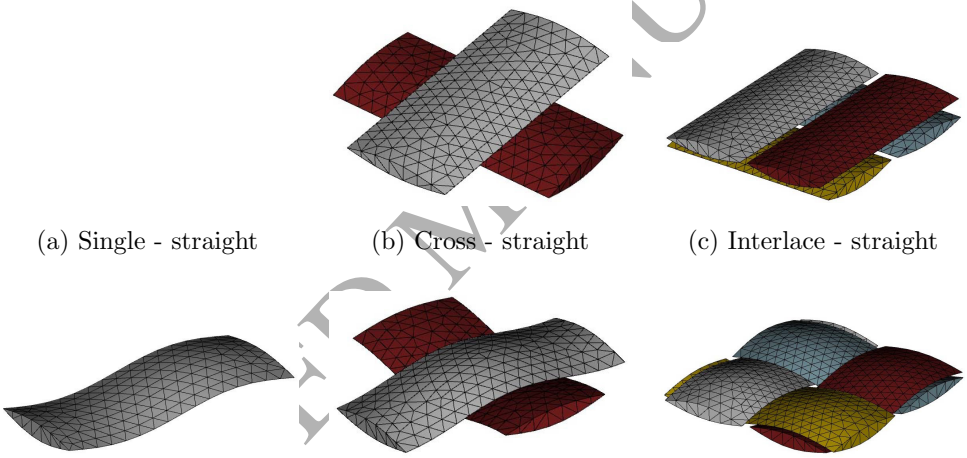

(a) Single - straight (b) Cross - straight (c) Interlace - straight

(d) Single - crimp (e) Cross - crimp (f) Interlace - crimp

Figure 5: Architecture of reinforcement

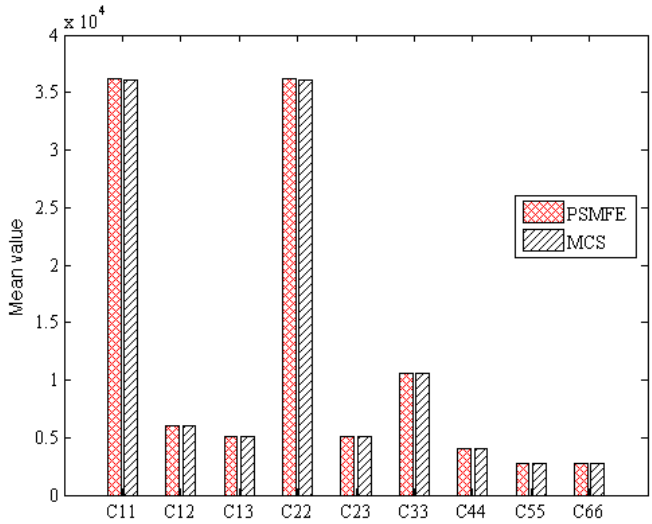

Figure 6: Estimated mean values of components of effective elastic tensor under E_z variation

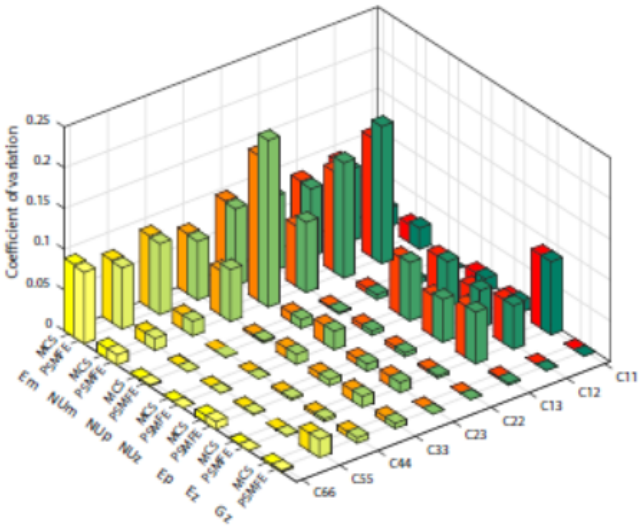

Figure 7: Comparisons between MCS and PSMFE on the estimates of CVs of components of effective elastic tensor due to variation in material properties

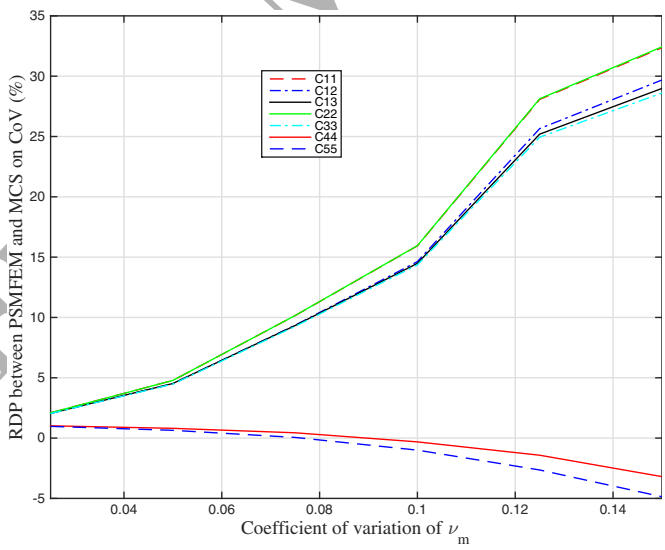

Figure 8: Relative percentage difference for CVs of components of effective elastic tensor due to variation of ν_m

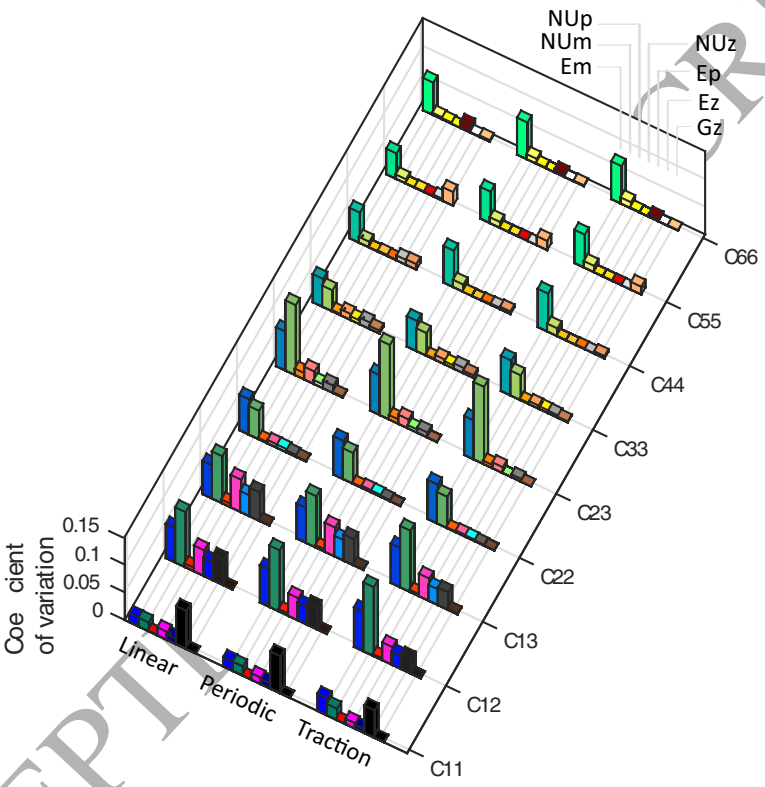

Figure 9: Sensitivity of CVs of components of effective elastic tensor with respect to variation of various material properties

	No. of degrees of freedom
Vertices	1
Edges	p - 1
Faces	(p - 2)(p - 1)/2
Interiors	(p - 3)(p - 2)(p - 1)/6

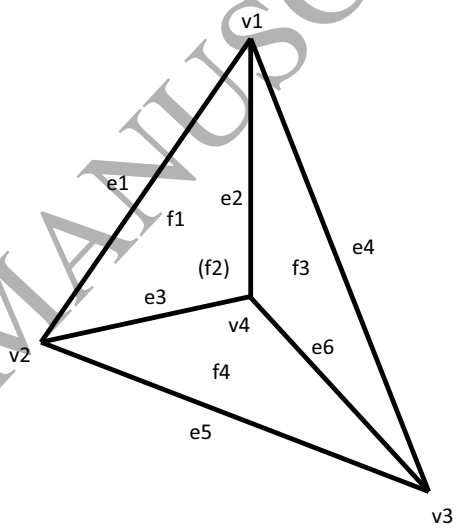

Figure 10: Hierarchical finite element - an example of tetrahedral element

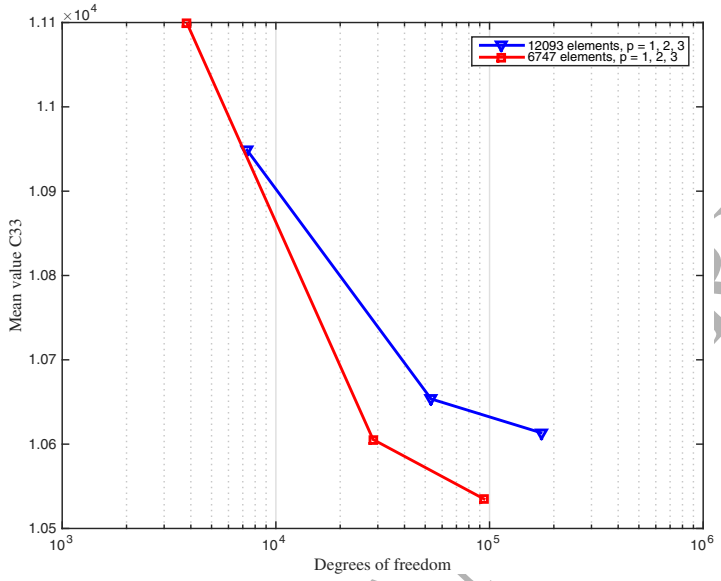

(a) Mean value

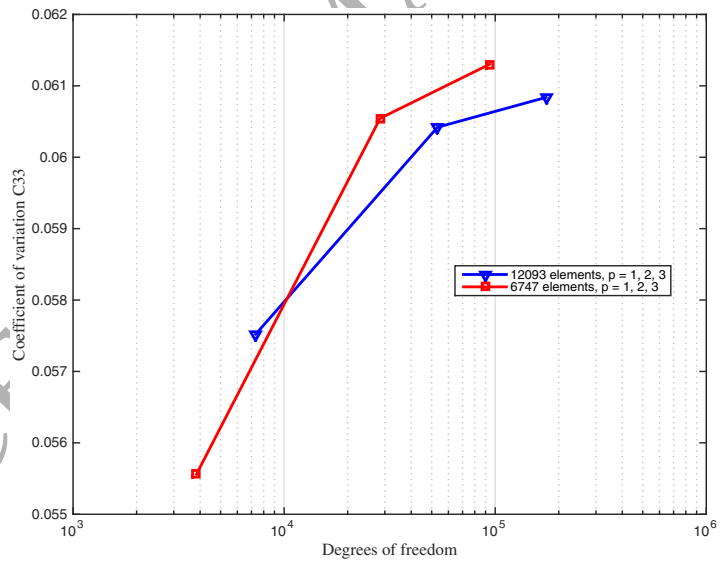

(b) Coefficient of variation

Figure 11: Efficiency of the p-version FE

Appendix A. Engineering constants

The stress-strain relations in xyz coordinate system are

$$\begin{Bmatrix} \varepsilon_x \\ \varepsilon_y \\ \varepsilon_z \\ \varepsilon_{xy} \\ \varepsilon_{xz} \\ \varepsilon_{yz} \end{Bmatrix} = \bar{\mathbf{S}} \begin{Bmatrix} \sigma_x \\ \sigma_y \\ \sigma_z \\ \sigma_{xy} \\ \sigma_{xz} \\ \sigma_{yz} \end{Bmatrix} \tag{A.1}$$

where $\bar{\mathbf{S}}$ is the effective compliance matrix, which is the inverse of the effective elastic matrix, $\bar{\mathbb{C}}$, in Eq. (35).

Under uniaxial loading, σ_x, Eq. (A.1) can be written as

$$\varepsilon_x = \bar{S}_{11}\sigma_x$$
$$\varepsilon_y = \bar{S}_{12}\sigma_x$$
$$\varepsilon_z = \bar{S}_{13}\sigma_x$$

The effective Young's modulus in x-direction is

$$E_x \equiv \frac{\sigma_x}{\varepsilon_x} = \frac{1}{\bar{S}_{11}} \tag{A.2}$$

The effective Poisson's ratio, ν_{xy} and ν_{xz}, are

$$\nu_{xy} \equiv -\frac{\varepsilon_y}{\varepsilon_x} = -\frac{\bar{S}_{12}}{\bar{S}_{11}}$$
$$\nu_{xz} \equiv -\frac{\varepsilon_z}{\varepsilon_x} = -\frac{\bar{S}_{13}}{\bar{S}_{11}}$$

Similarly, other effective engineering properties can be derived by applying uniaxial loading in the y and z directions, respectively, and pure shear

on the various coordinate planes. The results are summarized as follows:

$$
\begin{aligned}
E_y &= \frac{1}{\bar{S}_{22}} \\
\nu_{yx} &= -\frac{\bar{S}_{12}}{\bar{S}_{22}} \\
\nu_{yz} &= -\frac{\bar{S}_{23}}{\bar{S}_{22}} \\
E_z &= \frac{1}{\bar{S}_{33}} \\
\nu_{zx} &= -\frac{\bar{S}_{13}}{\bar{S}_{33}} \\
\nu_{zy} &= -\frac{\bar{S}_{23}}{\bar{S}_{33}} \\
G_{xy} &= \frac{1}{\bar{S}_{44}} \\
G_{xz} &= \frac{1}{\bar{S}_{55}} \\
G_{yz} &= \frac{1}{\bar{S}_{66}}
\end{aligned}
\tag{A.3}
$$